The Astrophysical Journal, 842:105 (7pp), 2017 June 20 https://doi.org/10.3847/1538-4357/aa7209

The Identification of the White Dwarf Companion to the Millisecond Pulsar J2317+1439

S. Dai[1], M. C. Smith[2], S. Wang[3], S. Okamoto[2], R. X. Xu[4], Y. L. Yue[3], and J. F. Liu[3]
[1] CSIRO Astronomy and Space Science, Australia Telescope National Facility, Box 76, Epping, NSW 1710, Australia; shi.dai@csiro.au
[2] Shanghai Astronomical Observatory, Chinese Academy of Sciences, Shanghai 200030, China
[3] National Astronomical Observatories, Chinese Academy of Sciences, Beijing 100012, China
[4] School of Physics and Kavli Institute for Astronomy and Astrophysics, Peking University, Beijing 100871, China
Received 2016 June 22; revised 2017 May 2; accepted 2017 May 6; published 2017 June 20

Abstract

We report the identification of the optical counterpart to the companion of the millisecond pulsar J2317+1439. At the timing position of the pulsar, we find an object with $g = 22.96 \pm 0.05$, $r = 22.86 \pm 0.04$, and $i = 22.82 \pm 0.05$. The magnitudes and colors of the object are consistent with a white dwarf (WD). Compared with WD cooling models, we estimate that it has a mass of $0.39^{+0.13}_{-0.10}\ M_{\odot}$, an effective temperature of 8077^{+550}_{-470} K, and a cooling age of 10.9 ± 0.3 Gyr. Combining our results with published constraints on the orbital parameters obtained through pulsar timing, we estimate the pulsar mass to be $3.4^{+1.4}_{-1.1}\ M_{\odot}$. Although the constraint on the pulsar mass is still weak, there is a significant possibility that the pulsar could be more massive than two solar masses.

Key words: pulsars: general – stars: individual (PSR J2317+1439) – white dwarfs

1. Introduction

Millisecond pulsars (MSPs) are a special subgroup of radio pulsars, with shorter spin periods and much smaller spin-down rates compared to "normal" pulsars. Most MSPs have low-mass white dwarf (WD) companions, and their fast spins are believed to be a result of mass transfer from the progenitor of the WD, known as recycling (e.g., Tauris 2011). Measuring the masses of MPSs and their companions allows us to study these systems in detail and learn about their formation, evolution, and the accretion process. Mass measurements of pulsars also enable constraints to be placed on the state of ultra-dense matter (Demorest et al. 2010; Antoniadis et al. 2013), and together with radio observations, they can be used to test general relativity (e.g., Kramer et al. 2006; Shao 2014). Precise masses of MSPs and their companions can be determined through high-precision pulsar timing by measuring the Shapiro delay, but this is possible in only exceptional cases. An alternative way to achieve this relies on combined optical and radio timing observations (e.g., van Kerkwijk et al. 1996). For WD companions that are bright enough for optical spectroscopy, a comparison of their spectrum with WD atmosphere models can determine the effective temperature and surface gravity. These can then be compared to WD evolutionary models to obtain their masses. The mass ratio can be determined through pulsar timing and/or spectroscopy of the WD (using the amplitude of the radial-velocity curve), which can then be combined with the WD mass to reveal the pulsar mass (e.g., van Kerkwijk et al. 2005).

PSR J2317+1439 is a 3.4 ms pulsar in a 2.46 day orbit (Camilo et al. 1993). The extremely low eccentricity of this binary system allows for a tight test of the local Lorentz invariance of gravity (Bell et al. 1996). Through long-term pulsar timing, the parallax of this pulsar has been measured to be 0.7 ± 0.2 mas (Matthews et al. 2016). Shapiro delay effects caused by the companion have been observed through high-precision pulsar timing of the MSP, but these are weak and produce relatively poor constraints on the masses of the companion and the MSP (Fonseca et al. 2016).

Previously, the companion to PSR J2317+1439 has not been reliably identified. Mignani et al. (2014) reported an association between the pulsar and a faint Sloan Digital Sky Survey (SDSS) source, J231709.23+143931.2, which has the following magnitudes: $u > 23.3$, $g = 22.95 \pm 0.16$, $r = 23.09 \pm 0.25$, $i > 22.9$, and $z > 25.5$. However, because this object is so faint, the SDSS photometry has large uncertainties; hence, it is difficult to ascertain the nature of the source. In this paper, we report our optical identification of the companion to PSR J2317+1439 with the Canada–France–Hawaii Telescope (CFHT). We estimate the temperature, the age, and the mass of the companion based on WD cooling models and constrain the possible mass of the MSP. The identification of the companion opens up the prospect of optical spectroscopy, which leads to precise mass measurements for both the MSP and the WD. In turn, this could lead to more stringent tests of gravity theories and new constraints on the equation of state of pulsars.

Details of the observations and data analysis are given in Section 2. We estimate the mass of WD and pulsar in Section 3. A summary of our results and discussions are given in Section 4.

2. Observational Data

2.1. Observations and Data Reduction

We used the MegaCam on CFHT to take *g*-, *r*-, and *i*-band images of a 1×1 square degree field containing PSR J2317+1439. This CFHT program (12BS08; PI: S. Dai) was applied through the Chinese Telescope Access Program.[5] The data were taken from 2012 July 15–20 for the three bands, with an additional *g*-band observation in September 17 of that year. The total exposure time was 1000, 2400, and 4300 s for the *g*-, *r*-, and *i*-bands, respectively, with observations between $0\farcs8$ to $1\farcs0$. Each filter's observation was split into multiple exposures to avoid saturation of bright stars, and dithered slightly between exposures to span the gaps between chips and to correct for bad pixels.

The data were pre-processed at CFHT with the Elixir pipeline[6] to correct for the instrumental signature across the whole mosaic. The pre-processed data were then processed at

[5] http://info.bao.ac.cn/tap/
[6] http://www.cfht.hawaii.edu/Instruments/Imaging/MegaPrime/

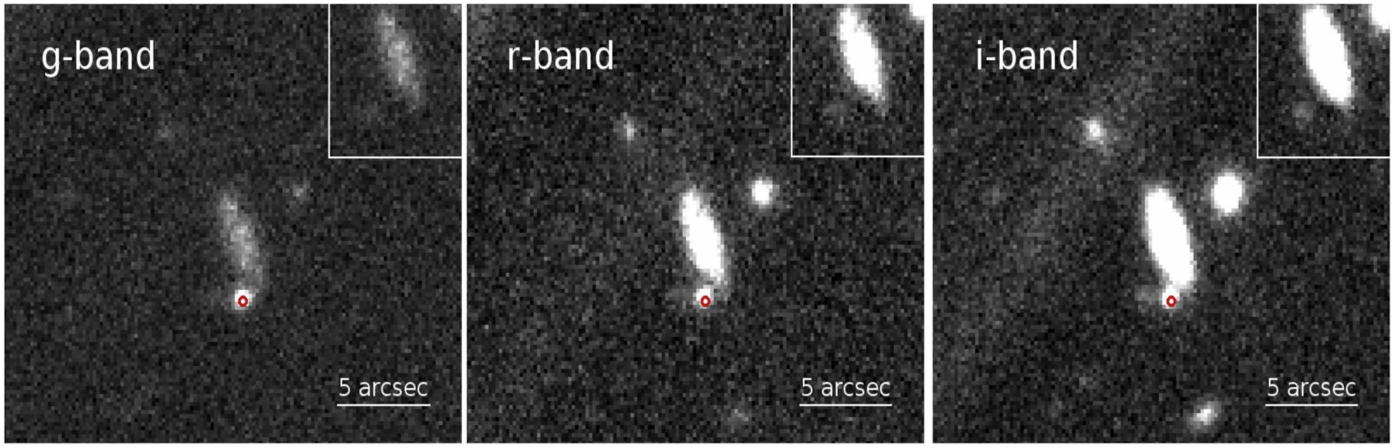

Figure 1. Cutouts showing our CFHT data around the location of PSR J2317+1439. The timing position of the MSP is marked with a red circle, and the radius corresponds to our astrometric uncertainty (0.″2). Cutouts of the PSF subtracted images are shown in the upper right corner for each band. The grayscale of each image shows the same luminosity range. Note that the faint diffuse diagonal bands in some of these images are a ghost from a nearby bright star.

Terapix[7] with a pipeline that has been used for the CFHT Legacy Survey.[8] The initial photometric calibrations were derived with *Scamp* (Bertin 2006) using the Ninth SDSS Data Release (DR9). An astrometric calibration was performed as a part of the pipeline[9] using the 2MASS catalog. The resulting astrometric uncertainties are 0.″23 in R.A. and 0.″21 in decl. using 1515 bright objects identified in both our images and in the 2MASS catalog. Once aligned astrometrically, exposures were rescaled and co-added by *Swarp* (Bertin et al. 2002) using the *Scamp* initial photometric rescaling. Subsections of the co-added images containing PSR J2317+1439 are shown in Figure 1.

2.2. Photometry

We performed point-spread function (PSF) photometry of the candidate MSP companion star, as well as of the field stars, using the co-added images. This was done using the DAOPHOT II package (Stetson 1994), which is distributed as a part of the IRAF software environment. We first used task *daofind* to obtain a coordinate list of detected objects through the analysis of the co-added images. Then, we performed aperture photometry with task *phot*. Task *pstselect* was used to select 300 isolated, bright, unsaturated stars across the field, and task *psf* was used to produce reliable PSF models for images of all three bands. We set *varorder* = 2 to allow the PSF model to vary over the image. PSF-fitting photometry was then performed with task *allstar* to obtain magnitudes and errors of objects in the list.

We recalibrated the photometry against SDSS DR9, fitting for the zero points with 423, 580, and 708 isolated, unsaturated ($17 < m_{\rm sdss} < 20$) point sources (sharpness parameter $|sh| < 0.5$) selected in the *g*-, *r*-, and *i*-bands, respectively. There was a clear dependence of the $m_{\rm sdss}$–$m_{\rm cfht}$ residuals on CFHT colors, most significantly in the *g*-band (for which the residual was as much as 0.1 mag). To correct such color dependences, we used transformations based on Sesar et al. (2011). For the *g*- and *r*-band magnitudes we used Equations (7) and (8) of Sesar et al. (2011)[10], but kept the constant terms as a free parameter. To determine the value of this term for each band, we fitted the medians of $m_{\rm sdss}$–$m_{\rm cfht}$ for our cross-matched stars. The best-fit values for the constant terms were −0.127 and −0.045 for the *g*- and *r*-bands, respectively. We found that the *i*-band residuals were not well fit by the relation from Sesar et al. (2011), and so we fit those ourselves using a quadratic polynomial. The best-fit polynomials gave us the following transformations, where $g'r'i'$ and *gri* correspond to uncalibrated and calibrated magnitudes, respectively:

$$g = g' - 0.127 - 0.062 \times (g' - r') + 0.365 \times (g' - r')^2 - 0.159 \times (g' - r')^3, \quad (1)$$

$$r = r' - 0.045 + 0.275 \times (g' - r') - 0.380 \times (g' - r')^2 + 0.163 \times (g' - r')^3, \quad (2)$$

$$i = i' + 0.042 - 0.078 \times (r' - i') + 0.041 \times (r' - i')^2. \quad (3)$$

In the left panels of Figure 2, we show the uncorrected $m_{\rm sdss}$–$m_{\rm cfht}$ residuals, where $m_{\rm sdss} = g^*, r^*, i^*$ are the SDSS magnitudes and $m_{\rm cfht} = g', r', i'$ are the uncalibrated CFHT magnitudes. Black points show the median of residuals and blue lines represent the best-fit polynomials. In the right panels, we show the color dependence corrected residuals and their medians, where $m_{\rm cfht} = g, r, i$ are the corrected CFHT magnitudes.

The scatter in the $m_{\rm sdss}$–$m_{\rm cfht}$ residuals is around 0.05–0.1 mag, which is larger than the internal errors and indicates that there are systematic uncertainties remaining in our photometry. To account for this, we first iteratively clipped 3σ outliers and calculated the standard deviations of $m_{\rm sdss}$–$m_{\rm cfht}$ residuals in each band ($\sigma_{\rm res}$). This dispersion is a combination of the systematic uncertainties ($\sigma_{\rm sys}$) together with the internal

[7] http://terapix.iap.fr/
[8] http://www.cfht.hawaii.edu/Science/CFHTLS/
[9] http://terapix.iap.fr/cplt/T0007/doc/T0007-doc.html

[10] Note that the cubic terms are missing from Equations (7) and (8) of Sesar et al. (2011); these should be −0.15920082 and +0.16278071 for (7) and (8), respectively (B. Sesar 2017, private communication).

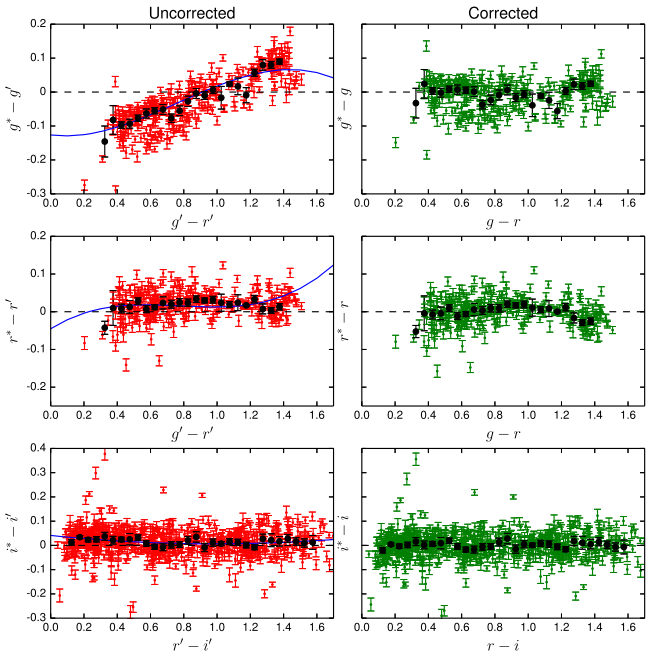

Figure 2. Dependence of the $m_{\rm sdss}$–$m_{\rm cfht}$ residuals on CFHT color. Left panels show the uncorrected residuals, and right panels show the corrected results. Black points represent the median of residuals, and blue lines show the best-fit polynomials.

uncertainties from our CFHT data ($\sigma_{\rm cfht}$) and from SDSS ($\sigma_{\rm sdss}$), i.e., the systematic uncertainty can be approximated by

$$\sigma_{\rm sys} = \sqrt{\sigma_{\rm res}^2 - \sigma_{\rm cfht}^2 - \sigma_{\rm sdss}^2}. \quad (4)$$

These systematic uncertainties are listed in Table 1 for each band.

2.3. Identification of the Optical Companion to PSR J2317+1439

We identified an optical object at the timing position of the MSP in all three bands. The optical position is $\alpha_{\rm J2000} = 23^{\rm h}17^{\rm m}09\overset{\rm s}{.}24$ and $\delta_{\rm J2000} = 14°39'31\overset{''}{.}46$, with an uncertainty of around $0\overset{''}{.}2$ in each coordinate coming from the astrometric calibration. The timing and astrometric parameters of the MSP are listed in Table 1 (Desvignes et al. 2016; Matthews et al. 2016), and the offset with our detection is around $0\overset{''}{.}24$, i.e., consistent with the uncertainty in the astrometric calibration. The reference epoch of astrometric parameters is MJD = 55,000, and the offsets introduced by pulsar proper motions at epochs of our optical observations are $\Delta\alpha \approx -4.2$ mas and $\Delta\delta \approx 10.7$ mas, which are negligible compared with astrometric uncertainties of the optical position. The astrometry of our detection also agrees with that of the SDSS object identified by Mignani et al. (2014). For objects with $g < 24$ mag, CFHT images have an average stellar density of six stars per square arcminute, which translates to only a 0.02% probability of a chance coincidence within an error circle with a radius of $0\overset{''}{.}2$. In Figure 1, we show cutouts of the CFHT images, with the timing position of the MSP marked as a red circle with a radius of $0\overset{''}{.}2$.

As can be seen from these images there is a background galaxy lying close to our optical object. However, this should not affect our photometry because the object is clearly resolved in all bands and we used PSF photometry.

Table 1
Parameters of PSR J2317+1439 and Photometric Results of the Companion

Timing Parameters (Desvignes et al. 2016)	
$P_{\rm s}$ (ms)	3.445251125644 88(18)
$\dot{P}_{\rm s}$ (10^{-20} s s^{-1})	0.2433(3)
τ (10^9 year)	15.6
Astrometric Parameters (Matthews et al. 2016)	
$\alpha_{\rm J2000}$	$23^{\rm h}17^{\rm m}09\overset{\rm s}{.}236644(9)$
$\delta_{\rm J2000}$	$+14°39'31\overset{''}{.}2557(2)$
μ_α	$-1.39(3)$ mas yr^{-1}
μ_δ	3.55(6) mas yr^{-1}
Parallax	0.7(2) mas
Orbital Parameters (Fonseca et al. 2016)	
$P_{\rm b}$	2.459331465 19(2) (days)
x	2.313943(4) (lt-s)
i	47^{+10}_{-7} (degree)
e	$5.7(16) \times 10^{-7}$

Photometric Results	g-band	r-band	i-band
Magnitudes	22.96 ± 0.02	22.86 ± 0.03	22.82 ± 0.03
$\sigma_{\rm sys}$	0.04	0.03	0.04
A_λ	0.185	0.128	0.095

Note. The timing, astrometric, and orbital parameters are from Desvignes et al. (2016), Matthews et al. (2016), and Fonseca et al. (2016). The extinction (A_λ) is estimated using models by Green et al. (2015) and coefficients from Schlafly & Finkbeiner (2011).

The distance to the pulsar is estimated to be $D_{\rm psr} = 1.3^{+0.4}_{-0.3}$ kpc based on the parallax measurement. We used the Bayesian approach described in Equation (22) of Igoshev et al. (2016). As summarized in the lower part of Table 1 from Igoshev et al. (2016), the priors assume a pulsar density distribution[11] from Lorimer et al. (2006), luminosity function from Faucher-Giguère and Kaspi (2006), and we take the flux to be 4 ± 1 mJy at 1.4 GHz (Kramer et al. 1998).

The magnitudes of the optical object are listed in Table 1. Note that these magnitudes are after applying the color-dependent correction described in Section 2.2, but before applying any extinction correction. Using models by Green et al. (2015), we obtained a reddening $E(B-V)$ of 0.056 ± 0.03 mag for a distance of 1.3 kpc toward PSR J2317+1439. Combined with the $R_{\rm V} = 3.1$ extinction law and coefficients for SDSS filters from Schlafly & Finkbeiner (2011), the g-, r-, and i-band extinctions are estimated and given in Table 1.

The dereddened color–magnitude and color–color diagrams are presented in Figure 3. The absolute magnitudes are estimated using $D_{\rm psr} = 1.3^{+0.4}_{-0.3}$ kpc, and the corresponding uncertainties are dominated by the distance uncertainties. Most WD companions to MSPs are known to be low-mass helium-core WDs with masses below 0.2–0.3 $M_\odot$ (e.g., van Kerkwijk et al. 2005) and are called extremely low-mass (ELM) WDs. In Figure 3, we compare our magnitudes and colors with theoretical evolutionary tracks for ELM WD models, covering

[11] Note that Table 1 of Igoshev et al. (2016) does not use the same scale-height as the reported reference (Lorimer et al. 2006). We use the value directly from Lorimer et al. (2006), which is $h = 0.33$ kpc.

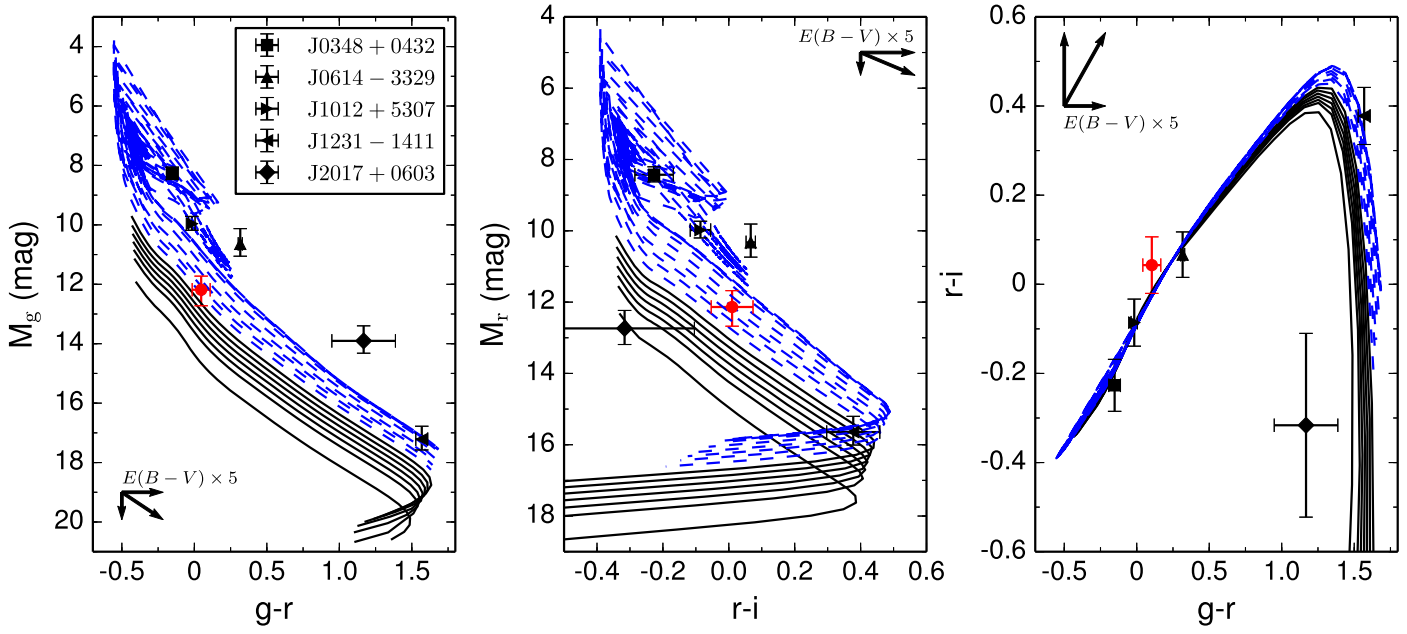

Figure 3. Color–magnitude diagrams and color–color diagram. In the magnitude–color diagrams, absolute magnitudes (estimated using $D_{\rm psr} = 1.3^{+0.4}_{-0.3}$ kpc) are shown as red points with error bars. Solid black lines show CO-core WD models, with masses varying linearly from 0.5 to 1.2 $M_\odot$. Dashed blue lines show ELM WD models from Althaus et al. (2013), with masses varying linearly from 0.1554 to 0.4352 $M_\odot$. Magnitudes and colors of the companions to PSRs J0348+0432, J0614−3329, J1012+5307, J1231−1411, and J2017+0603 are shown as black points with error bars. For PSR J2317+1439, the estimated reddening is $E(B-V) = 0.056 \pm 0.03$ mag, and we have included the reddening vector on each panel (scaled up by a factor of five for clarity).

WD masses from ∼0.16 to 0.44 $M_\odot$. The ELM WD cooling models come from Althaus et al. (2013)[12], where theoretical luminosities and temperatures have been transformed into absolute magnitudes by applying bolometric corrections for pure hydrogen model atmospheres (provided by P. Bergeron; see Holberg & Bergeron 2006; Bergeron et al. 2011). MSPs with more massive WD companions (e.g., PSR J1614−2230; Demorest et al. 2010) have also been found and are proposed to evolve from intermediate-mass X-ray binaries (e.g., Tauris et al. 2011). Therefore, we also consider evolutionary tracks for carbon–oxygen (CO) core WDs with pure hydrogen model atmospheres, covering WD masses from 0.5 to 1.2 $M_\odot$. These models are from Holberg & Bergeron (2006), Kowalski & Saumon (2006), Tremblay et al. (2011), and Bergeron et al. (2011).[13]

The magnitudes and colors of our source are in good agreement with the ELM models, but lie at the low-mass side of the CO-core WD models. Although the colors of the object are also consistent with other blue stars, such as blue horizontal branch or blue straggler stars, the magnitudes would imply a distance of many kiloparsecs, in which case it could not be associated with the pulsar. For comparison, in Figure 3, we also presented magnitudes and colors of the companions to PSRs J0348+0432 (Antoniadis et al. 2013), J0614−3329 (Bassa et al. 2016), J1012+5307 (Nicastro et al. 1995), J1231−1411 (Bassa et al. 2016), and J2017+0603 (Bassa et al. 2016).[14] Extinctions have been corrected following the same procedure as for PSR J2317+1439.

[12] http://evolgroup.fcaglp.unlp.edu.ar/TRACKS/tracks_heliumcore.html

[13] See http://www.astro.umontreal.ca/~bergeron/CoolingModels/ for more details about cooling models and color calculations.

[14] Apparent magnitudes of the companions to PSRs J0348+0432 and J1012+5307 were obtained from the Sloan Digital Sky Survey (York et al. 2000) website (http://skyserver.sdss.org/dr13/). For PSRs J0614−3329, J1231−1411, and J2017+0603, the distances are not well constrained, and we used distances estimated from dispersion measures (Bassa et al. 2016) and assumed 20% uncertainties (Cordes & Lazio 2002).

3. Estimating the Mass of the Companion and Pulsar

Since we have both the colors and distance to the companion, we can use models to constrain the mass, temperature, and age of the WD. We have done this by constructing a single composite model that uses the ELM tracks for the mass range 0.1554–0.4352 $M_\odot$ and CO-core tracks for the mass range 0.5–1.2 $M_\odot$. We interpolated these models in the mass–temperature plane using natural neighbor interpolation with the IDL command "griddata."

Assuming Gaussian errors on the photometry, the likelihood of any given model point is described by the following equation:

$$\mathcal{L} = \prod_{f=g,r,i} \frac{1}{\sqrt{2\pi\delta_f^2}} \exp\left(\frac{-(m_f - m_f^{\rm model})^2}{2\delta_f^2}\right), \quad (5)$$

where m_f and δ_f are the apparent magnitude and error for our observed bands $f = g, r, i$ and the model is a function of the unknown parameters (in our case, effective temperature, WD mass, and distance). We calculated the likelihood using this equation for each point in our 2D interpolated plane, taking a 4000 × 4000 grid linearly spaced in the temperature range 6000–10,000 K and in the mass range 0.1554–1.2 $M_\odot$.

As outlined in Section 2.3, we have used Equation (22) of Igoshev et al. (2016) to estimate the pulsar distance; we use the resulting probability distribution function as a prior in Equation (5). We correct our magnitudes for extinction, as discussed in Section 2.3, and incorporate the 0.03 mag uncertainty on the reddening in our modeling. We used uniform priors on both effective temperature and WD mass. The resulting constraints on the effective temperature and WD mass are shown in Figure 4. We obtained a WD mass of $0.39^{+0.13}_{-0.10}$ $M_\odot$, an effective temperature of 8077^{+550}_{-470} K, and a

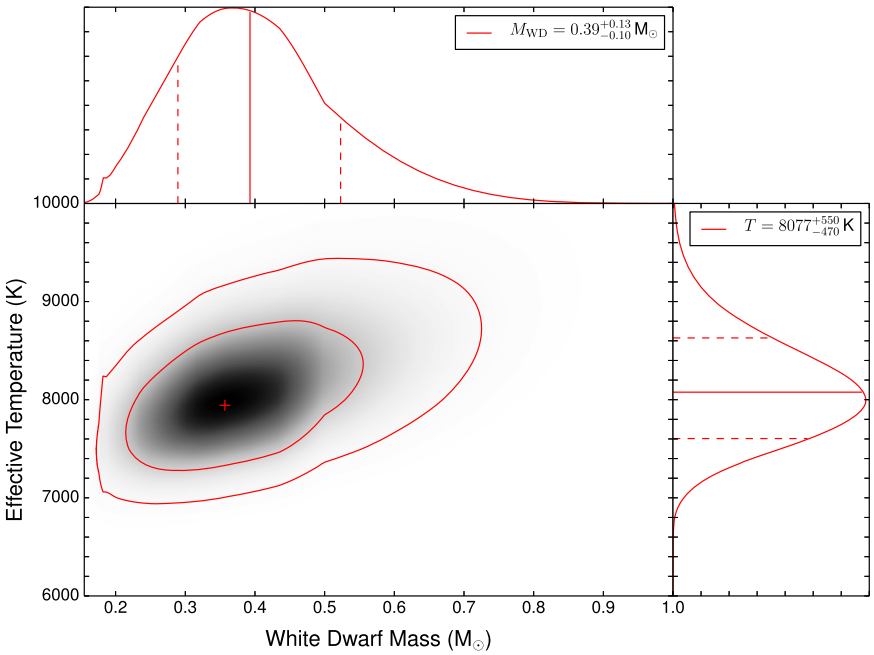

Figure 4. Constraints on the WD mass and effective temperature from the CFHT photometry using the composite ELM and the CO-core WD models. The contours correspond to 1σ and 2σ confidence intervals, and the peak is denoted by a cross. The marginalized 1D likelihoods are presented in the top and side panels, with the solid and dashed lines showing the median and 1σ confidence intervals, respectively.

cooling age of 10.9 ± 0.3 Gyr, where we have quoted the median of the probability distribution and the 1σ error.

Our constraints on the WD mass can be used to further constrain the pulsar mass through the equation

$$\frac{(m_{\rm WD}\sin i)^3}{(m_{\rm PSR}+m_{\rm WD})^2} = \frac{4\pi^2}{G}\frac{x^3}{P_{\rm b}^2}, \quad (6)$$

where i is the inclination angle, x is the projected semimajor axis, and $P_{\rm b}$ is the orbital period. The most up-to-date estimates for the orbital parameters, which have been presented in Table 1, come from pulsar timing (Fonseca et al. 2016). For PSR J2317+1439 the timing analysis leads to only weak constraints on the WD mass and, consequently, the pulsar mass. In Figure 5, we show how the timing confidence intervals (grayscale and dashed contours) contract if we apply a prior based on our photometric constraints on the WD mass (solid contours). We can use these new constraints on the inclination and WD mass to estimate the NS mass through Equation (6). The NS mass is now better constrained, with a 1σ confidence interval of $3.4^{+1.4}_{-1.1}\,M_\odot$ (see Figure 6). Although this is still not a very tight constraint, it is indicative that the pulsar may be massive, with probabilities of only 9% that the mass is below $2\,M_\odot$.

Previous studies have argued that the system of PSR J2317+1439 has evolved from a low-mass binary and has a helium-core WD companion (van Kerkwijk et al. 2005). The relation of WD mass to orbital period for systems evolved from low-mass binaries has been studied by a number of authors (e.g., Tauris & Savonije 1999; Lin et al. 2011; Istrate et al. 2016). For orbital periods larger than 2 days, previous studies gave very similar relations, which have been shown to agree well with MSP binary systems with low-mass helium-core WD companions (see, for example, Figure 8 of Fonseca et al. 2016). For the 2.3 day orbital period of PSR J2317+1439, assuming a helium-core WD companion, the Tauris & Savonije (1999) models predict a WD mass of 0.21–0.23 $M_\odot$, where the spread comes from the uncertainty in the chemical abundance of the WD. If we apply a Gaussian prior to the WD mass, with mean 0.22 and standard deviation 0.01 $M_\odot$, the resulting pulsar mass is $1.58 \pm 0.14\,M_\odot$. The WD mass predicted by Tauris & Savonije (1999) is inconsistent at 1σ with our result. However,

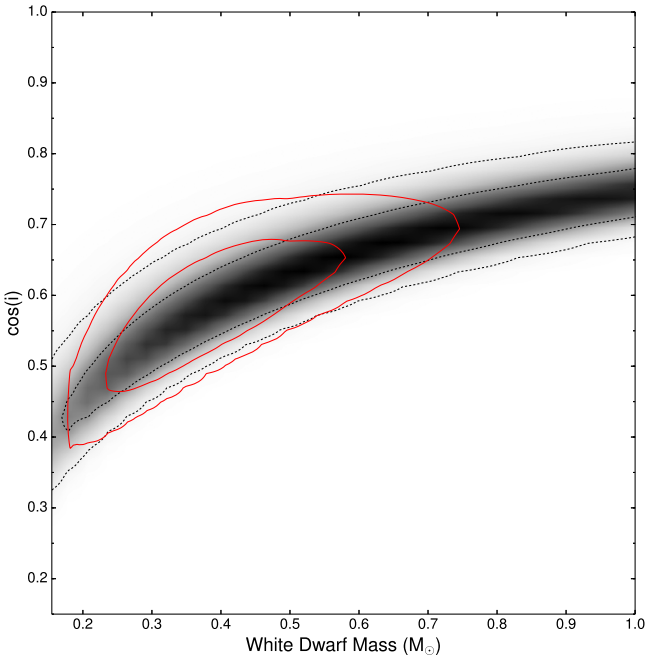

Figure 5. Constraints on the WD mass and inclination angle of the binary system. The grayscale and dashed contours correspond to the constraints derived from PSR timing (Fonseca et al. 2016), while the solid contours show the constraints after applying a prior on the WD mass derived from our CFHT photometry and WD models.

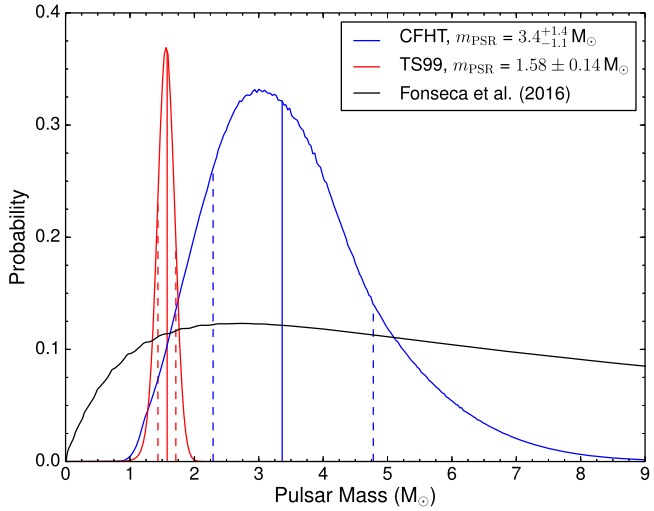

Figure 6. Constraints on the mass for PSR J2317+1439. Each curve is normalized so that the area underneath is unity, except the red curve which has been scaled down by a factor of six. The vertical solid and dashed lines denote the median and 1σ confidence intervals, respectively.

the current constraint on the pulsar parallax is not particularly tight, and this is important because the WD mass is degenerate with its absolute magnitudes. To obtain a WD mass of 0.22 $M_\odot$, the distance would need to be 1.94 kpc, although this is outside the 1σ constraint obtained in Section 2.3, a more precise measurement of the parallax would clearly reduce the uncertainty.

4. Conclusion and Discussion

We have reported the optical identification of the companion to PSR J2317+1439. The timing position of the pulsar agrees with the optical position of the detection and the photometry agrees with WD cooling models. This identification opens up the possibility of precisely measuring the WD temperature and surface gravity through optical spectroscopy, although the faint nature of the star means that this will require large optical telescopes. Combined with high-precision pulsar timing, this would lead to a precise mass measurement for the MSP.

By fitting the photometry with WD models, we have estimated the mass of the WD to be $0.39^{+0.13}_{-0.10}$ $M_\odot$ and the effective temperature to be 8077^{+550}_{-470} K. The WD models predict a cooling age of 10.9 ± 0.3 Gyr, which is close to the characteristic age of the pulsar of 15.6 Gyr. These estimates depend on the distance to the system, which can be obtained from the trigonometric parallax measurement. Since the parallax is not very well constrained (0.7 ± 0.2 mas), the Lutz–Kelker bias needs to be corrected for (e.g., Verbiest et al. 2012), and we have incorporated the correction into our estimates following the Bayesian approach described in Igoshev et al. (2016).

It has been suggested that this system has evolved from a low-mass binary, and the companion is likely to be a helium-core WD (van Kerkwijk et al. 2005). Although our results agree with such a scenario, the WD mass of $0.39^{+0.13}_{-0.10}$ $M_\odot$ is marginally inconsistent with predictions based on the relation of WD mass to orbital period. For the 2.46 day orbital period, models from Tauris & Savonije (1999) predict a WD mass of 0.21–0.23 $M_\odot$, which is just outside the 1σ confidence interval obtained from fitting our photometry with WD models. Therefore, the nature of the progenitor binary and how it evolved during the mass-exchanging X-ray phase are still unclear.

Combining our WD mass estimate with constraints on the orbital parameters of this system derived from pulsar timing (Fonseca et al. 2016), we have estimated the pulsar mass to be $3.4^{+1.4}_{-1.1}$ $M_\odot$. This is consistent with the mass measured by Fonseca et al. (2016), but with much smaller uncertainties. Although tentative, our results indicate that PSR J2317+1439 may be an extremely massive neutron star ($>2.04\,M_\odot$ at 90% confidence). If confirmed, this could challenge our understanding of the state of dense matter and structure of neutron stars (e.g., Xu & Guo 2017). Long-term high-precision timing of PSR J2317+1439 could in principle better measure the Shapiro delay and then the mass of both WD and pulsar, but this is limited by the timing precision we can achieve for this pulsar. However, further observations could also lead to an improved parallax measurement and this would improve our WD mass estimate. For example, if the parallax error was reduced by a factor of two to 0.1 mas, then the corresponding pulsar mass uncertainty would be reduced by around 25%. An alternative way to do this is to obtain an optical spectrum of the WD, as discussed previously. If one could measure the surface gravity of the WD, this would dramatically reduce the allowed range of parameter space and provide much tighter constraints on the pulsar mass.

The authors wish to thank E. Fonseca for providing his likelihood distributions from pulsar timing, P. Bergeron for providing bolometric corrections, and S. Justham for helpful comments. This research uses data obtained through the Telescope Access Program (TAP), which has been funded by the National Astronomical Observatories of China, the Chinese Academy of Sciences (the Strategic Priority Research Program "The Emergence of Cosmological Structures" Grant No. XDB09000000), and the Special Fund for Astronomy from the Ministry of Finance. M.C.S. acknowledges financial support from the CAS One Hundred Talent Fund, the National Key Basic Research Program of China 2014CB845700, and from NSFC grants 11173002 and 11333003. R.X.X. acknowledges support from NSFC grants 11673002 and U1531243. This work is based on data products produced at the TERAPIX data center located at the Institut d'Astrophysique de Paris. We thank all the people that have made this AASTeX what it is today. This includes but not limited to Bob Hanisch, Chris Biemesderfer, Lee Brotzman, Pierre Landau, Arthur Ogawa, Maxim Markevitch, Alexey Vikhlinin, and Amy Hendrickson.

References

Althaus, L. G., Miller Bertolami, M. M., & Córsico, A. H. 2013, A&A, 557, A19
Antoniadis, J., Freire, P. C. C., Wex, N., et al. 2013, Sci, 340, 448
Bassa, C. G., Antoniadis, J., Camilo, F., et al. 2016, MNRAS, 455, 3806
Bell, J. F., Camilo, F., & Damour, T. 1996, ApJ, 464, 857
Bergeron, P., Wesemael, F., Dufour, P., et al. 2011, ApJ, 737, 28
Bertin, E. 2006, in ASP Conf. Ser. 351, Astronomical Data Analysis Software and Systems XV, ed. C. Gabriel et al. (San Francisco, CA: ASP), 112
Bertin, E., Mellier, Y., Radovich, M., et al. 2002, in ASP Conf. Ser. 281, Astronomical Data Analysis Software and Systems XI, ed. D. A. Bohlender, D. Durand, & T. H. Handley (San Francisco, CA: ASP), 228
Camilo, F., Nice, D. J., & Taylor, J. H. 1993, ApJL, 412, L37

Cordes, J. M., & Lazio, T. J. W. 2002, arXiv:astro-ph/0207156
Demorest, P. B., Pennucci, T., Ransom, S. M., Roberts, M. S. E., & Hessels, J. W. T. 2010, Natur, 467, 1081
Desvignes, G., Caballero, R. N., Lentati, L., et al. 2016, MNRAS, 458, 3341
Faucher-Giguère, C.-A., & Kaspi, V. M. 2006, ApJ, 643, 332
Fonseca, E., Pennucci, T. T., Ellis, J. A., et al. 2016, ApJ, 832, 167
Green, G. M., Schlafly, E. F., Finkbeiner, D. P., et al. 2015, ApJ, 810, 25
Holberg, J. B., & Bergeron, P. 2006, AJ, 132, 1221
Igoshev, A., Verbunt, F., & Cator, E. 2016, A&A, 591, A123
Istrate, A. G., Marchant, P., Tauris, T. M., et al. 2016, A&A, 595, A35
Kowalski, P. M., & Saumon, D. 2006, ApJL, 651, L137
Kramer, M., Stairs, I. H., Manchester, R. N., et al. 2006, Sci, 314, 97
Kramer, M., Xilouris, K. M., Lorimer, D. R., et al. 1998, ApJ, 501, 270
Lin, J., Rappaport, S., Podsiadlowski, P., et al. 2011, ApJ, 732, 70
Lorimer, D. R., Faulkner, A. J., Lyne, A. G., et al. 2006, MNRAS, 372, 777
Matthews, A. M., Nice, D. J., Fonseca, E., et al. 2016, ApJ, 818, 92
Mignani, R. P., Corongiu, A., Pallanca, C., et al. 2014, MNRAS, 443, 2223
Nicastro, L., Lyne, A. G., Lorimer, D. R., et al. 1995, MNRAS, 273, L68
Schlafly, E. F., & Finkbeiner, D. P. 2011, ApJ, 737, 103
Sesar, B., Jurić, M., & Ivezić, Ž. 2011, ApJ, 731, 4
Shao, L. 2014, PhRvL, 112, 111103
Stetson, P. B. 1994, PASP, 106, 250
Tauris, T. M. 2011, in ASP Conf. Ser. 447, Evolution of Compact Binaries, ed. L. Schmidtobreick, M. R. Schreiber, & C. Tappert (San Francisco, CA: ASP), 285
Tauris, T. M., Langer, N., & Kramer, M. 2011, MNRAS, 416, 2130
Tauris, T. M., & Savonije, G. J. 1999, A&A, 350, 928
Tremblay, P.-E., Bergeron, P., & Gianninas, A. 2011, ApJ, 730, 128
van Kerkwijk, M. H., Bassa, C. G., Jacoby, B. A., & Jonker, P. G. 2005, in ASP Conf. Ser. 328, Binary Radio Pulsars, ed. F. A. Rasio & I. H. Stairs (San Francisco, CA: ASP), 357
van Kerkwijk, M. H., Bergeron, P., & Kulkarni, S. R. 1996, ApJL, 467, L89
Verbiest, J. P. W., Weisberg, J. M., Chael, A. A., Lee, K. J., & Lorimer, D. R. 2012, ApJ, 755, 39
Xu, R., & Guo, Y. 2017, in Centennial of General Relativity, ed. C. A. Zen Vasconcellos (Singapore: World Scientific), 119
York, D. G., Adelman, J., Anderson, J. E., Jr., et al. 2000, AJ, 120, 1579